Lattice Boltzmann method for non-Newtonian (power-law) fluids

Susana Gabbanelli
Departamento de Matemática y Grupo de Medios Porosos, Facultad de Ingeniería, Universidad de Buenos Aires, Buenos Aires, Argentina

German Drazer* and Joel Koplik†
Benjamin Levich Institute and Department of Physics, City College of the City University of New York, New York 10031, USA
(Received 29 June 2005; published 25 October 2005)

We study an *ad hoc* extension of the lattice Boltzmann method that allows the simulation of non-Newtonian fluids described by generalized Newtonian models. We extensively test the accuracy of the method for the case of shear-thinning and shear-thickening truncated power-law fluids in the parallel plate geometry, and show that the relative error compared to analytical solutions decays approximately linear with the lattice resolution. Finally, we also tested the method in the reentrant-flow geometry, in which the shear rate is no longer a scalar and the presence of two singular points requires high accuracy in order to obtain satisfactory resolution in the local stress near these points. In this geometry, we also found excellent agreement with the solutions obtained by standard finite-element methods, and the agreement improves with higher lattice resolution.

DOI: 10.1103/PhysRevE.72.046312 PACS number(s): 47.11.+j, 47.50.+d, 47.10.+g, 02.70.Rr

I. INTRODUCTION

Since its origin, more than 15 years ago, the lattice Boltzmann method (LBM) has proved to be a powerful numerical technique for the simulation of single- and multiphase fluid flows in complex geometries. In fact, the LBM has been successfully applied to different problems in fluid dynamics and the interest in the method has grown rapidly in recent years. The LBM is particularly suited for complex geometries and interfacial dynamics, and its initial applications included transport in porous media and multiphase and multicomponent fluid flows [1]. It was then adapted by Ladd and others to simulate particle-fluid suspensions [2]. It has also been applied to high Reynolds number incompressible flows and turbulence, and the implementation of thermal and compressible schemes is being actively pursued [3]. Viscoelastic fluids, for various constitutive models, have also been successfully modeled with the LBM [4,5]. One advantage of the LBM is that data communications between nodes is always local, which makes the method extremely efficient for large-scale, massively parallel computations (see Ref. [6] for an interesting discussion on the LBM capabilities compared to the existing continuum-based computational fluid dynamics methods). Another property of the LBM that has lately attracted considerable attention is the microscopic origin of its mesoscopic kinetic equations, which could therefore readily incorporate molecular level interactions. This makes the LBM very compelling for microscale fluid dynamics in microfluidic devices [7] which typically present noncontinuum and surface-dominated effects (e.g., high Knudsen number conditions, electrokinetic and wetting phenomena). This microscopic-based approach also makes the LBM a good candidate for hybrid, multiscale simulations of fluid flows.

However, the extension of the LBM to (inelastic) non-Newtonian fluids has received limited attention so far, in spite of the fact that a reliable LBM for this type of non-Newtonian flow would be very valuable; for instance, in studies of transport in geological porous media, an area in which the LBM has been extensively applied [8–10] due to its simple implementation in complex geometries. In addition to geological systems, the flow of non-Newtonian fluids is commonly found in many areas of science and technology.

In this work, we study an *ad hoc* modification of the LBM, first introduced by Aharonov and Rothman [11], in which the local value of the viscosity depends on the strain-rate tensor. We show that this modification to the LBM accurately describes the flow of truncated power-law fluids, both shear thinning and shear thickening, not only in unidirectional flows (parallel plates geometry) but also in two-dimensional flows with simultaneous shear components in more than one direction (reentrant corner geometry).

II. LATTICE BOLTZMANN METHOD

The LBM can be viewed as an implementation of the Boltzmann equation on a discrete lattice and for a discrete set of velocity distribution functions [12],

$$f_i(\mathbf{x}+\mathbf{e}_i\Delta x, t+\Delta t) = f_i(\mathbf{x},t) + \Omega_i(f(\mathbf{x},t)), \tag{1}$$

where f_i is the particle velocity distribution function along the ith direction, $\Omega_i(f(\mathbf{x},t))$ is the *collision operator* which takes into account the rate of change in the distribution function due to collisions, and Δx and Δt are the space and time step discretizations, respectively [1]. Then, the density ρ and momentum density $\rho\mathbf{u}$ are given by the first two moments of the distribution functions,

*Present address: Department of Chemical & Biomolecular Engineering, Johns Hopkins University, 3400 North Charles Street, Baltimore, Maryland 21218. Electronic address: drazer@mailaps.org
†Electronic address: koplik@sci.ccny.cuny.edu

$$\rho = \sum_i f_i, \quad \rho \mathbf{u} = \sum_i f_i \mathbf{e}_i, \tag{2}$$

where we assumed that the discretization is consistent with the Boltzmann equation, $\mathbf{x}+\mathbf{e}_i$ corresponding to the nearest neighbors of the point $\mathbf{x}$. Note that in the previous equation, and in the remainder of the article, all quantities are rendered dimensionless using Δx and Δt as the characteristic space and time scales, respectively. Also note that, as we are concerned with incompressible flows, we do not need to introduce a dimension of mass.

A. Bhatnagar-Gross-Krook approximation

Assuming that the system is close to equilibrium the collision operator is typically linearized about a local equilibrium distribution function f_i^{eq}, and assuming further that the local particle distribution relaxes to equilibrium with a single characteristic (relaxation) time τ, we arrive at the Bhatnagar, Gross, and Krook approximation of the LBM [1],

$$f_i(\mathbf{x} + \mathbf{e}_i \Delta x, t + \Delta t) = f_i(\mathbf{x}, t) + \frac{f_i(\mathbf{x}, t) - f_i^{eq}(\mathbf{x}, t)}{\tau}, \tag{3}$$

where the relaxation time τ is directly related to the kinematic viscosity of the fluid $\nu=(2\tau-1)/6$.

B. Non-Newtonian flows

The *ad hoc* extension of the LBM proposed by Aharonov and Rothman [11] to simulate non-Newtonian fluids consists of determining the value of the relaxation time τ locally, in such a way that the desired local value of the viscosity is recovered. The viscosity is related to the local rate of strain through the constitutive equation for the stress tensor. A commonly used model of (inelastic) non-Newtonian fluids is the *generalized Newtonian* model, in which the relation between the stress tensor σ_{ij} and the rate-of-strain tensor D_{ij} is similar to that for Newtonian fluids, $\sigma_{ij}=2\mu D_{ij}$, but with μ a function of the invariants of the local rate-of-strain tensor, $\mu=\mu(D_{ij})$. In particular, we are interested in the widely used power-law model [13] $\mu=m\dot{\gamma}^{n-1}$, where $n>0$ is a constant characterizing the fluid. The case $n<1$ corresponds to shear-thinning (pseudoplastic) fluids, whereas $n>1$ corresponds to shear-thickening (dilatant) fluids, and $n=1$ recovers the Newtonian behavior. The magnitude of the local shear rate $\dot{\gamma}$ is related to the second invariant of the rate-of-strain tensor, $\dot{\gamma}=\sqrt{D_{ij}D_{ij}}$, where the components of the rate-of-strain tensor D_{ij} are computed locally from the velocity field. In particular, after obtaining the instantaneous velocity field from the LBM we then compute D_{ij} from a first-order finite-difference approximation to the local derivatives of the velocity.

However, there is an obvious obstacle to a direct implementation of the power-law fluid in the LBM, in that the effective viscosity diverges for zero shear rates ($\dot{\gamma}=0$) in a shear-thinning fluid ($n<1$). Analogously, the viscosity becomes zero for a shear-thickening fluid at zero shear rates. In previous studies it is not clear how this problem was avoided.

Clearly, both limits are unphysical and, in fact, it is known that many non-Newtonian fluids exhibit a power-law behavior only in some range of shear rates, and a constant viscosity is observed outside that range [13]. Here, we used the simplest model of such fluids: the *truncated power-law* model,

$$\nu(\dot{\gamma}) = \mu(\dot{\gamma})/\rho = \begin{cases} m\dot{\gamma}_0^{(n-1)}, & \dot{\gamma} < \dot{\gamma}_0, \\ m\dot{\gamma}^{(n-1)}, & \dot{\gamma}_0 < \dot{\gamma} < \dot{\gamma}_\infty, \\ m\dot{\gamma}_\infty^{(n-1)}, & \dot{\gamma} > \dot{\gamma}_\infty. \end{cases} \tag{4}$$

Using the truncated power-law model has an additional advantage in the LBM. It is well known that the LBM can accurately simulate viscous flows only in a limited range of kinematic viscosities. The method becomes unstable for relaxation times close to $\tau \gtrsim 1/2$ [14] (small kinematic viscosities, $\nu \lesssim 0.001$) and its accuracy is very poor for $\tau \gtrsim 1$ [15] (relatively large kinematic viscosities, $\nu \gtrsim 1/6$). Therefore, we set the lower and upper saturation values of the kinematic viscosity in Eq. (4) to $\nu_{min}=0.001$ and $\nu_{max}=0.1$. It is clear that the maximum value of the viscosity corresponds to the value at zero shear rate for shear-thinning fluids ($n<1$), whereas the opposite is true for shear-thickening materials ($n>1$). Note that setting the value of the maximum model viscosity to $\nu_{max}=0.1$ for a given maximum fluid viscosity ν_{max}^* and a spatial resolution Δx simply corresponds to choosing a particular value of the time step in order to satisfy $\nu_{max}^*=\nu_{max}(\Delta x^2/\Delta t)$ [6]. Since the kinematic viscosity scales with $\Delta x^2/\Delta t$, to keep the dimensionless viscosity constant as we increase the number of lattice nodes N, we shall rescale Δt according to the previous relationship, that is, since $\Delta x \propto 1/N$ then $\Delta t \propto 1/N^2$. In what follow we use the three-dimensional face-centered-hypercubic projection model of the LBM with 19 velocities (D3Q19 following the notation in Ref. [16]).

III. FLOW BETWEEN PARALLEL PLATES

We first test the proposed LBM for non-Newtonian flows in a simple unidirectional flow, the flow between two parallel plates separated a distance b in the z direction (Hele-Shaw cell) in the presence of a pressure gradient in the x direction. We use periodic boundary conditions in both x and y directions. The resulting flow field is unidirectional, with $v_x(z)$ the only nonzero velocity component, the rate of strain is a scalar function of the local velocity, $\dot{\gamma}=|dv_x/dz|$, and the Navier-Stokes equations are greatly simplified [17].

In order to compute the exact solution to the Navier-Stokes equations for a pressure driven flow of a truncated power-law fluid in the Hele-Shaw geometry we split the system into (in principle) three different regions. We shall describe the solutions obtained in the regions between $z=0$ and $b/2$ and the analogous solutions for $z>b/2$ follow by symmetry. The first region we consider is the high shear-rate region close to the walls, *region H* for $z<z_h$, in which the shear rate exceeds $\dot{\gamma}_\infty$, and the fluid is Newtonian with effective kinematic viscosity $\nu_\infty=m\dot{\gamma}_\infty^{(n-1)}$; the second one is the intermediate region in which the fluid behaves as a power

law according to Eq. (4), *region I* for $z_h<z<z_l$; and the last one is the low shear-rate region close to the center of the channel, *region L* for $z_l<z<b/2$, in which the shear rate is lower than $\dot{\gamma}_0$ and the fluid is again Newtonian, but with kinematic viscosity $\nu_0=m\dot{\gamma}_0^{(n-1)}$. Matching then the solution obtained in each region with the conditions of continuity in the velocity and the stress, we obtain the general solution to the problem, in terms of the pressure gradient $G\rho=-\nabla P$,

$$v_x(z)=\begin{cases}\left(\dfrac{G}{2\nu_\infty}\right)z(b-z), & 0\leqslant z\leqslant z_h,\\ \dfrac{n}{n+1}\left(\dfrac{G}{m}\right)^{1/n}\left[\left(\dfrac{b}{2}\right)^{(n+1)/n}-\left(\dfrac{b}{2}-z\right)^{(n+1)/n}\right]+\alpha_1 & z_h\leqslant z\leqslant z_l,\\ \left(\dfrac{G}{2\nu_0}\right)z(b-z)+\alpha_2 & z_l\leqslant z\leqslant b/2,\end{cases} \tag{5}$$

with the constants α_1 and α_2 given by

$$\alpha_1=\left(\frac{G}{2\nu_\infty}\right)z_h(b-z_h)-\frac{n}{n+1}\left(\frac{G}{m}\right)^{1/n}\times\left[\left(\frac{b}{2}\right)^{(n+1)/n}-\left(\frac{b}{2}-z_h\right)^{(n+1)/n}\right],$$

$$\alpha_2=\frac{n}{n+1}\left(\frac{G}{m}\right)^{1/n}\left[\left(\frac{b}{2}\right)^{(n+1)/n}-\left(\frac{b}{2}-z_l\right)^{(n+1)/n}\right]-\left(\frac{G}{2\nu_0}\right)z_l(b-z_l)+\alpha_1, \tag{6}$$

and the transition points z_h and z_l,

$$z_h=\frac{b}{2}-\left(\frac{\nu_\infty}{m^{1/n}}\right)^{n/(n-1)}\frac{1}{G}=\frac{b}{2}-\frac{m\dot{\gamma}_\infty^n}{G},$$

$$z_l=\frac{b}{2}-\left(\frac{\nu_0}{m^{1/n}}\right)^{n/(n-1)}\frac{1}{G}=\frac{b}{2}-\frac{m\dot{\gamma}_0^n}{G}. \tag{7}$$

Clearly, the number of regions that coexist will depend on the magnitude of the imposed pressure gradient G. For very small pressure gradients $G\ll 1$, both z_h and z_l become negative (see the previous equation), which means that shear rates are smaller than $\dot{\gamma}_0$ across the entire gap and only region L exists. As G increases, there is a range of pressure gradients $m\dot{\gamma}_0^n<(b/2)G<m\dot{\gamma}_\infty^n$ for which $z_l>0$ but $z_h<0$, and therefore regions L and I coexist. Finally, for $G>(2/b)m\dot{\gamma}_\infty^n$ we obtain $z_h>0$, and all three regions are present in the flow. Note that for large values of G both transition points converge to the center of the cell, z_l, $z_h\to b/2$. Thus, Eq. (7) allows us to choose the appropriate value of G in order to investigate the different regimes.

We performed a large number of simulations for different values of the power-law exponent n. Specifically, we consider two shear-thinning fluids, $n=0.50$ and 0.75, and two shear-thickening fluids, $n=1.25$ and 2.00. In all cases we performed simulations for two different magnitudes of the external forcing: one for which the region of low shear rates L is important, that is, relatively small pressure gradients for which $z_l\sim b/4$; and a second one in which the fluid behaves as a power-law fluid almost in the entire gap, that is, $z_l\sim b/2$. In both cases the shear rate does not exceed $\dot{\gamma}_\infty$. In Fig. 1 we present a comparison between the lattice Boltzmann results and the analytical solution given in Eq. (5) for a shear-thinning fluid with power-law exponent $n=0.50$. The simulation corresponds to a relatively small pressure gradient for which the region of small shear-rates is large, $z_l\sim b/4$. Both regions, region L in which the fluid behaves as a Newtonian one, and region I in which the effective viscosity is a power law, are shown. The agreement with the analytical solution is excellent, with relative error close to 0.1%. In Fig. 2 we present a similar comparison between the LBM and the analytical solution, but for a shear-thickening fluid ($n=2.00$) which behaves as a power-law fluid across almost the entire channel. Again the agreement is excellent with relative error smaller than 0.1%.

Finally, for each of these cases we run a series of simulations in which the number of lattice nodes in the direction of the gap, N, was increased from 10 to 400, and computed the relative error of the LBM results compared to the analytical solutions, defined as $\Sigma_{i=1}^{N}(1-v_i^{LBM}/v_i^{anal})^2$. In order to obtain the accuracy of the LBM as a function of the number of nodes, we simulated the same physical problem but changed Δx from 1 to 0.025. In addition, since the accuracy of the LBM depends on the model viscosity, we also changed Δt according to $\Delta t=\Delta x^2$, so that the model viscosity remains the same, independent of the number of nodes. Then, in order to compare the velocity field always at the same physical time since startup, the number of time steps was increased inversely proportional to Δt (reaching $\sim 10^8$ time steps for $N=400$). In Fig. 3 we present the results obtained for the different fluids and different pressure gradients. It is clear that, in all cases, the relative error decreases, approximately as $1/N$, as the number of nodes is increased, and eventually becomes of the order of 0.1% (an arbitrary target accuracy that we set for our simulations). The error was found to be independent of the pressure gradient, or the size of the non-Newtonian region I, but strongly depends on the power-law

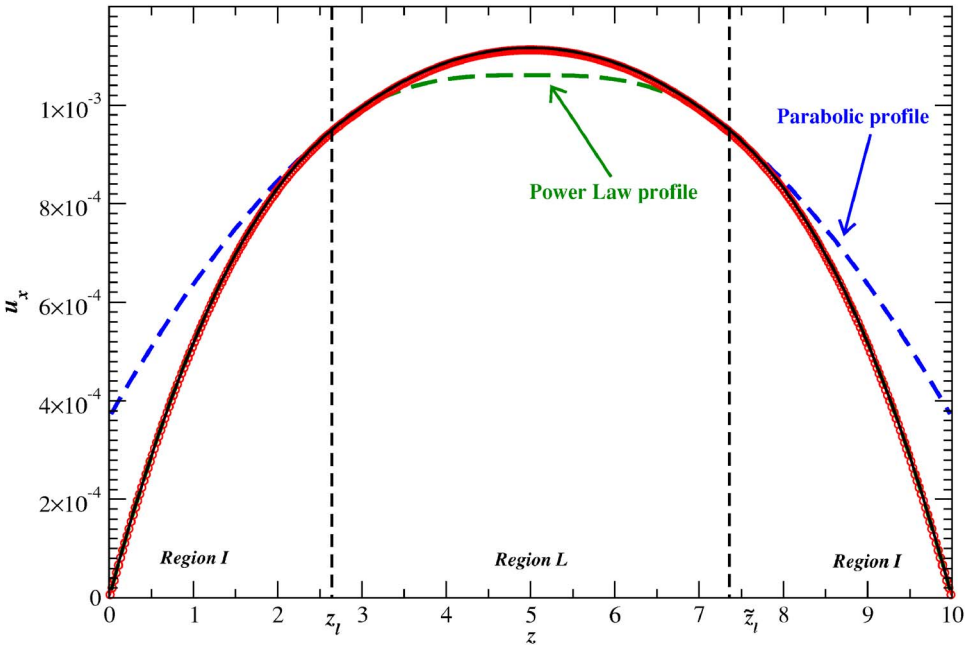

FIG. 1. (Color online) Comparison between a lattice Boltzmann simulation and the analytical solution for the flow between two parallel plates separated a distance $b=10$. The power-law exponent of the fluid is $n=0.50$ (shear thinning). The pressure gradient is $\nabla P=6\times10^{-6}$, $\rho=1$, $\nu_0=0.1$, $\nu_\infty=0.001$, $m=10^{-3}$, and $N=400$. The circles correspond to the lattice Boltzmann simulations. The solid line corresponds to the analytical solution given by Eq. (5). Also shown, in dashed lines, are the continuations of the Newtonian and power-law solutions outside their regions of applicability. The vertical, dashed lines correspond to the transition points, z_l and $\tilde{z}_l=b-z_l$, between the low shear-rate region L, and the region of intermediate shear rates, I.

exponent. In particular, the relative error seems to increase as the magnitude of $(1-n)/n$ increases, with the error in the Newtonian case $(n=1)$ decaying faster than $1/N$. This is probably related to the first-order finite-difference approximation used to compute the spatial derivatives of the fluid velocity which determine the local viscosity through Eq. (4). It would then be possible to improve the accuracy of the method by implementing a higher order approximation of the local shear-rates. Another possibility would be to use the constitutive equation [Eq. (4)] to obtain the local value of the viscosity in terms of the stress tensor, which, in turn, can be computed directly from the particle velocity distribution functions, f_i [1,3]. This latter approach has the advantage that it avoids computing the local derivatives of the velocity field.

IV. REENTRANT CORNER FLOW

In the previous section we tested the LBM for non-Newtonian fluids in a Hele-Shaw geometry and found excellent agreement with the analytical solutions as the number of nodes was increased. In that case, the flow is unidirectional and therefore the shear-rate is a scalar, which is a rather simple type of flow. In contrast, we shall now test the LBM in a more demanding geometry, that is, the *reentrant corner* geometry sketched in Fig. 4. In this case, the shear rate is no longer a scalar as in the Hele-Shaw geometry and, in addition, the presence of two singular points, located at the *entrant* and *reentrant* corners (see Fig. 4), requires high accuracy in order to obtain satisfactory stress resolution near

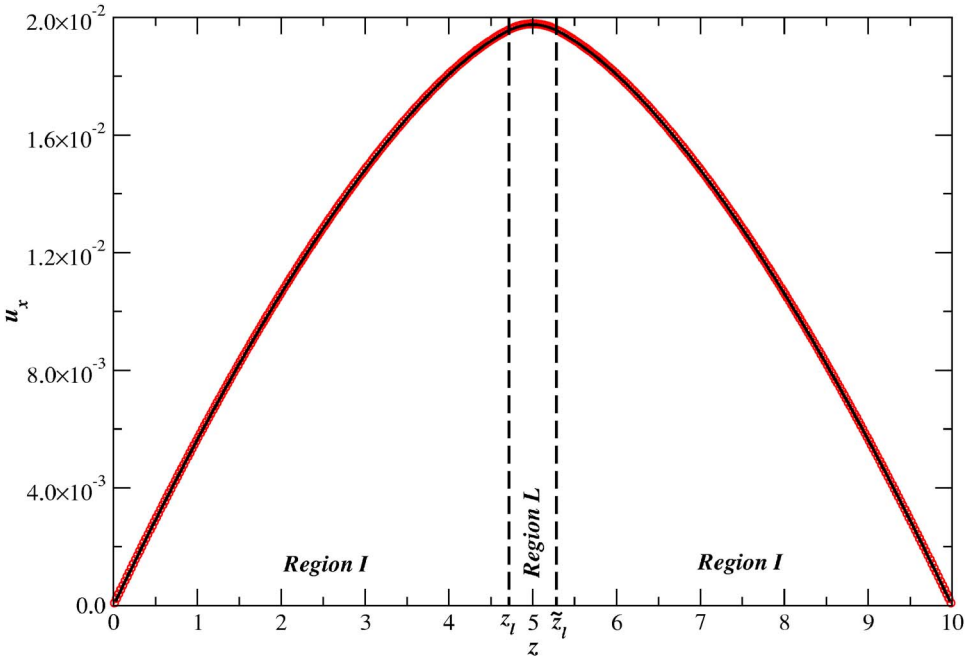

FIG. 2. (Color online) Comparison between a lattice Boltzmann simulation and the analytical solution for the flow between two parallel plates separated a distance $b=10$. The power-law exponent of the fluid is $n=2.00$ (shear thickening). The pressure gradient is $\nabla P=5\times10^{-6}$, $\rho=1$, $\nu_0=0.001$, $\nu_\infty=0.1$, $m=10^{-3}$, and $N=400$. The circles correspond to the lattice Boltzmann simulations and the solid line corresponds to the analytical solution given by Eq. (5). The vertical dashed lines correspond to the transition points z_l and $\tilde{z}_l=b-z_l$, between the low shear-rate region L and the intermediate shear-rate region I.

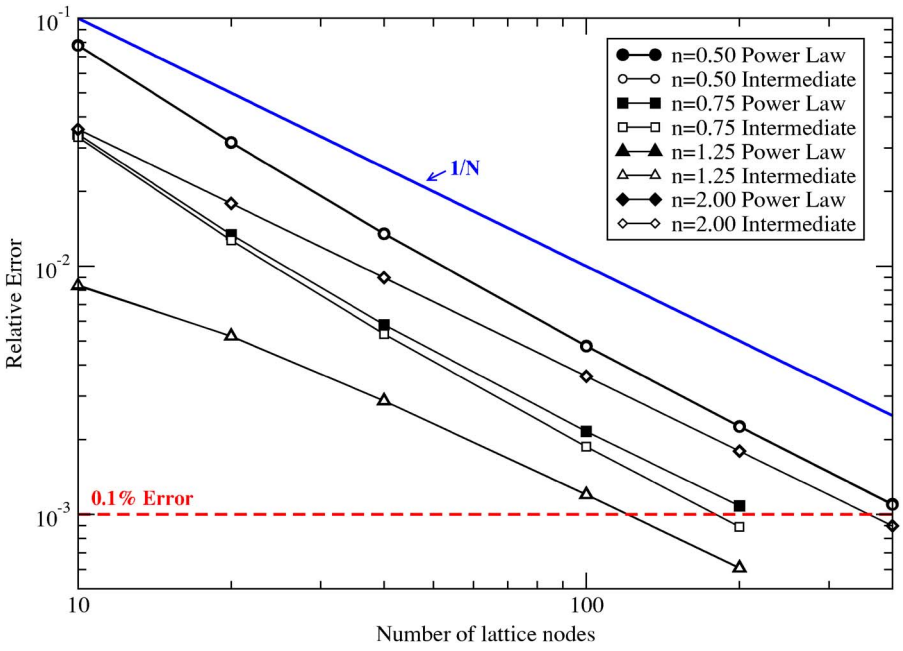

FIG. 3. (Color online) Relative error of the LBM compared to the analytical solution for the flow between parallel plates, as a function of the number of lattice points used in the simulations. The points correspond to simulations with the LBM for four different fluids, two shear-thinning fluids ($n=0.50$ and 0.75) and two shear-thickening fluids ($n=1.25$ and 2.00). For all fluids we also present results corresponding to two different regimes: one at high pressure gradients, in which the low shear-rate region, region L, is small (power law), and the other one at intermediate pressure gradients in which both regions L and I are comparable (note that with the exception of $n=0.75$ both regimes give almost exactly the same relative error and, in fact, the corresponding points overlap almost entirely). In all cases, we increased the lattice resolution until the relative error was on the order of 0.1%. The solid line shows the general trend of the data, $1/N$.

these points (although no analog to Moffatt's analysis is available for non-Newtonian fluids near wedges and corners, it is believed that nonintegrable stress singularities develop in this case, and numerical techniques do not always converge [18]). Motivated by these issues we simulated the flow in the reentrant corner geometry using the LBM for a shear-thinning fluid with power-law exponent $n=0.50$. In Fig. 4 we present the streamlines corresponding to the computed veloc-

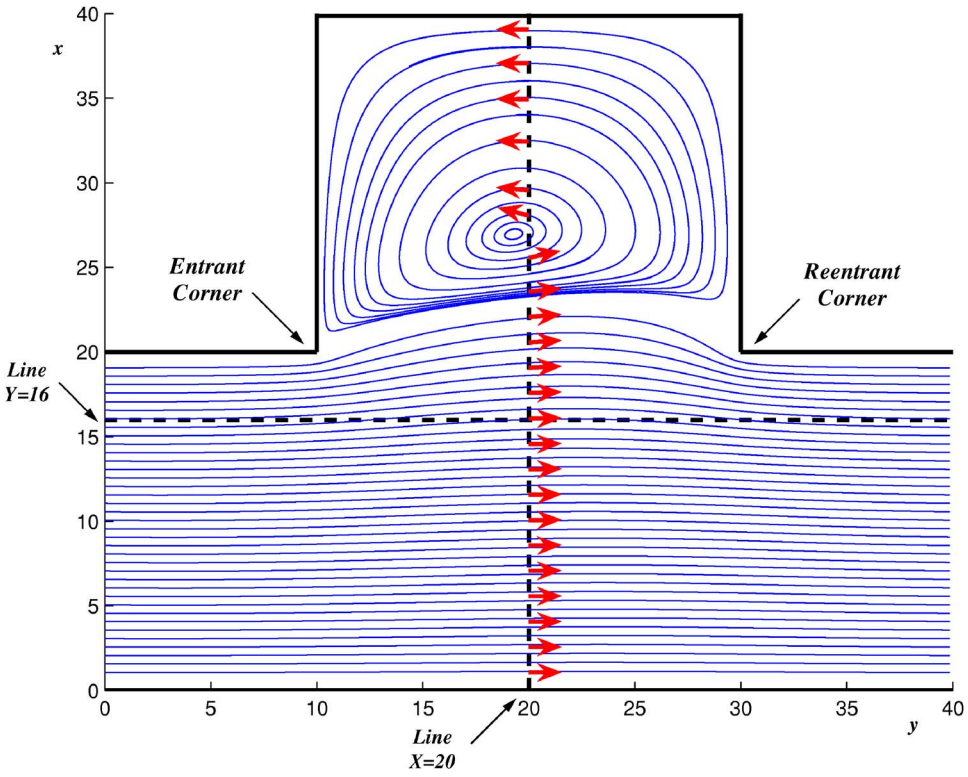

FIG. 4. (Color online) Streamlines in the reentrant flow geometry. The flow direction is shown at the center of the channel. Note the asymmetry due to inertia effects. The dashed lines show the lines in which we compare the solutions of the LBM method with the solutions obtained by finite-element calculations.

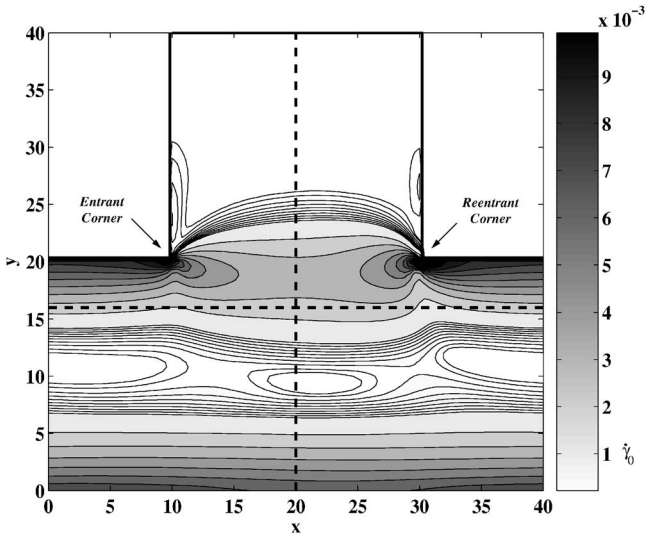

FIG. 5. Contour plot of the local magnitude of the shear rate, as computed with the LBM. The lowest level of the plot corresponds to $\dot{\gamma}_0$, that is, the fluid behaves as Newtonian in those regions. High shear rates, and accordingly high shear stresses, are localized at the entrant and reentrant corners.

ity field, obtained for a pressure gradient $\nabla P = 10^{-5}$, where the recirculation region inside the cavity can be observed (note that the separation between streamlines was chosen for visualization purposes only and it is not related to the local flow rate, since the magnitude of the fluid velocity sharply decays inside the cavity). The corresponding Reynolds number is Re=4, computed with the maximum viscosity ν_0, and the measured mean velocity. In fact, the streamlines shown in Fig. 4 are fore-aft asymmetric, due to inertia effects, which are absent in low Reynolds-number flows. We also computed the local magnitude of the shear rate, related to the local stress field through the constitutive relation given by Eq. (4). In Fig. 5 we present a contour plot of the magnitude of the shear rate in the reentrant corner geometry with the lowest level in the contour plot corresponding to $\dot{\gamma}_0$. It can be seen that the fluid is Newtonian in small regions at the center of the channel and inside the recirculation region. It is also clear that, as discussed before, both the entrant and reentrant corners are singular points where the shear rate increases to its highest values in the system.

Finally, in order to perform a more quantitative test of the LBM, we solved the problem numerically using the finite-element commercial software FIDAP (Fluent Inc.). In Figs. 6 and 7 we compare the solutions obtained with the LBM for different resolutions, ranging from $N=40\times40$ to $N=320\times320$, with the finite-element results obtained with FIDAP. The comparison is made along two lines, one oriented along the flow direction (dashed line at $Y=16$ in Fig. 4) and a second one oriented in the perpendicular direction (dashed line at $X=20$ in Fig. 4). In Fig. 6 we compare the velocity along the channel, u_x, in the line perpendicular to x that is located at the center of the system ($X=20$, see Fig. 4). A velocity profile similar to that in a Hele-Shaw cell is observed for $0<y\lesssim20$, as well as the recirculation flow inside the cavity (see the inset). In Fig. 7 we plot the velocity in the vertical direction, u_y, along a horizontal line close to the upper wall of the channel ($Y=16$, see Fig. 4). It is clear that there is some fluid penetration into the cavity (entrant flow) in the first half of the channel and some reentrant flow in the second half (note that, as mentioned before, the flow is not symmetric about $x=20$ due to inertia effects). In both cases we found an excellent agreement between the two methods, and the agreement clearly improved as the number of lattice nodes was increased in the LBM (the number of elements in the finite-element computations was fixed to 100×100).

V. CONCLUSIONS

We have extensively tested an *ad hoc* modification of the lattice Boltzmann method that extends its use to generalized Newtonian fluids, in which the non-Newtonian character of the fluids is modeled as an effective viscosity. Specifically,

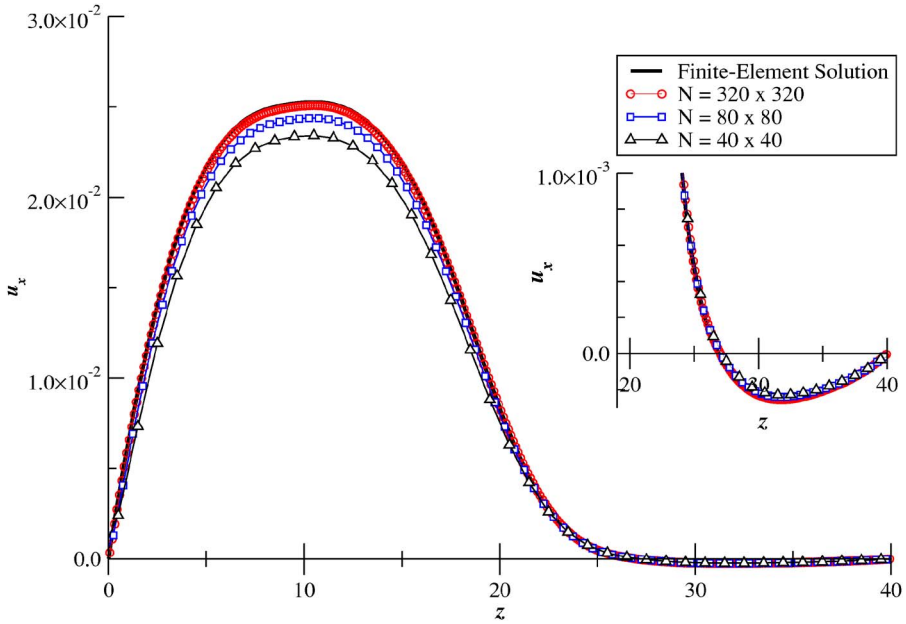

FIG. 6. (Color online) Velocity component along the channel, u_x, plotted in a line perpendicular to the flow (dashed line $X=20$ in Fig. 4). We compare the results of the finite-element calculations (solid line) with the results of the LBM (points) for different lattice resolutions. In the inset we plot the velocity profile inside the recirculation region.

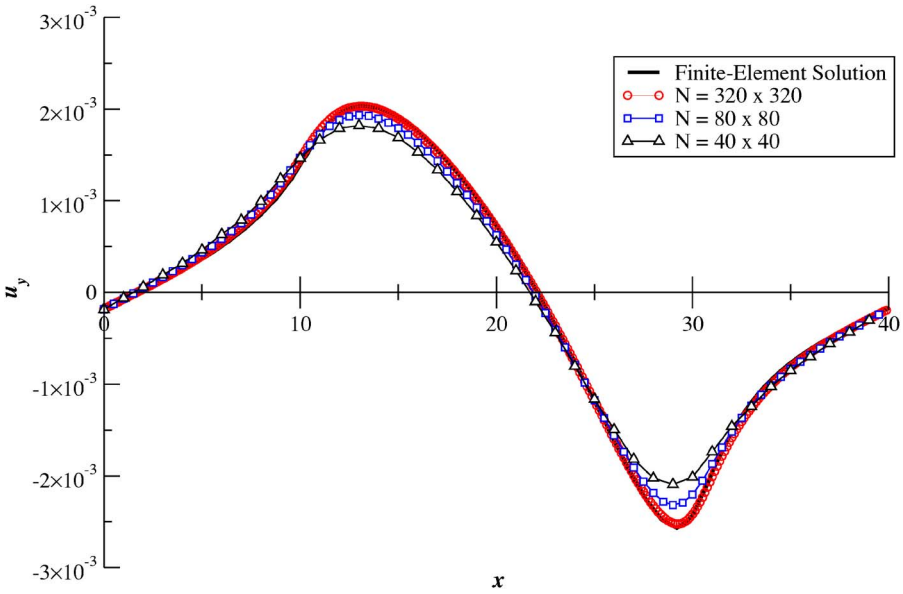

FIG. 7. (Color online) Velocity component perpendicular to the flow direction, u_y, plotted in a line parallel to the flow and close to the top wall of the channel (dashed line $Y=16$ in Fig. 4). We compare the results of the finite-element calculations (solid line) with the results of the LBM (points) for different lattice resolutions.

we calculated the accuracy of the method for truncated power-law fluids and showed that the relative error decays (linearly) as the resolution of the lattice (number of lattice points) is increased. The error was computed directly from the analytical solutions of the problem. The same trend was observed for both shear-thinning ($n<1$) and shear-thickening ($n>1$) fluids, as well as for intermediate and high shear rates. In all cases the relative error was of the order of 0.1% for the highest resolution employed. Finally, we also tested the method in the reentrant flow geometry and showed that it is in excellent agreement with the solution obtained by means of finite-element calculations. Again, the accuracy of the method was shown to increase with the number of lattice points.

ACKNOWLEDGMENTS

This work is part of a collaboration supported by the Office of International Science and Engineering of the National Science Foundation under Grant No. INT-0304781. This research was supported by the Geosciences Research Program, Office of Basic Energy Sciences, U.S. Department of Energy, and computational facilities were provided by the National Energy Resources Scientific Computer Center.

[1] S. Chen and G. D. Doolen, Annu. Rev. Fluid Mech. **30**, 329 (1998).
[2] A. J. C. Ladd and R. Verberg, J. Stat. Phys. **104**, 1191 (2001).
[3] D. Z. Yu, R. W. Mei, L. S. Luo, and S. Wei, Prog. Aerosp. Sci. **39**, 329 (2003).
[4] L. Giraud, D. D'Humieres, and P. Lallemand, Europhys. Lett. **42**, 625 (1998).
[5] I. Ispolatov and M. Grant, Phys. Rev. E **65**, 056704 (2002).
[6] R. R. Nourgaliev, T. N. Dinh, T. G. Theofanous, and D. Joseph, Int. J. Multiphase Flow **29**, 117 (2003).
[7] D. Raabe, Modell. Simul. Mater. Sci. Eng. **12**, R13 (2004).
[8] G. Drazer and J. Koplik, Phys. Rev. E **62**, 8076 (2000).
[9] G. Drazer and J. Koplik, Phys. Rev. E **63**, 056104 (2001).
[10] G. Drazer and J. Koplik, Phys. Rev. E **66**, 026303 (2002).
[11] E. Aharonov and D. H. Rothman, Geophys. Res. Lett. **20**, 679 (1993).
[12] D. H. Rothman and S. Zaleski, *Lattice-Gas Cellular Automata, Simple Models of Complex Hydrodynamics* (Cambridge University Press, Cambridge, U.K., 1997).
[13] R. B. Bird, W. E. Stewart, and E. N. Lightfoot, *Transport Phenomena*, 2nd ed. (Wiley Text Books, New York, 2001).
[14] X. D. Niu, C. Shu, Y. T. Chew, and T. G. Wang, J. Stat. Phys. **117**, 665 (2004).
[15] O. Behrend, R. Harris, and P. B. Warren, Phys. Rev. E **50**, 4586 (1994).
[16] Y. H. Qian, D. D'Humieres, and P. Lallemand, Europhys. Lett. **17**, 479 (1992).
[17] L. G. Leal, *Laminar Flow and Convective Transport Processes* (Butterworth-Heinemann, London, 1992).
[18] J. Koplik and J. R. Banavar, J. Rheol. **41**, 787 (1997).